Biosensors and Bioelectronics 146 (2019) 111765

Contents lists available at ScienceDirect

Biosensors and Bioelectronics

journal homepage: http://www.elsevier.com/locate/bios

Functionalized etched tilted fiber Bragg grating aptasensor for label-free protein detection

Marzhan Sypabekova [a,b,*], Sanzhar Korganbayev [a,1], Álvaro González-Vila [c], Christophe Caucheteur [c], Madina Shaimerdenova [a], Takhmina Ayupova [a], Aliya Bekmurzayeva [a,b], Luca Vangelista [d], Daniele Tosi [a,b]

[a] PI National Laboratory Astana, Laboratory of Biosensors and Bioinstruments, 53 Kabanbay Batyr Avenue, 010000, Nur-Sultan, Kazakhstan
[b] School of Engineering and Digital Sciences, Nazarbayev University, 53 Kabanbay Batyr Avenue, 010000, Nur-Sultan, Kazakhstan
[c] Electromagnetism and Telecommunication Department, University of Mons, Boulevard Dolez 31, 7000, Mons, Belgium
[d] School of Medicine, Nazarbayev University, 53 Kabanbay Batyr Avenue, 010000, Nur-Sultan, Kazakhstan

ARTICLE INFO

Keywords:
Optical fiber
Aptasensor
Thrombin
Etching
Detection

ABSTRACT

An aptasensor based on etched tilted fiber Bragg grating (eTFBG) is developed on a single-mode optical fiber targeting biomolecule detection. TFBGs were chemically etched using hydrofluoric acid (HF) to partially remove the fiber cladding. The sensor response was coarsely interrogated, resulting on a sensitivity increase from 1.25 nm/RIU (refractive index unit) at the beginning of the process, up to 23.38 nm/RIU at the end of the etching, for a RI range from 1.3418 to 1.4419 RIU. The proposed aptasensor showed improved RI sensitivity as compared to the unetched TFBG, without requiring metal depositions on the fiber surface or polarization control during the measurements. The proposed sensor was tested for the detection of thrombin-aptamer interactions based on silane-coupling surface chemistry, with thrombin concentrations ranging from 2.5 to 40 nM. Functionalized eTFBGs provided a competitive platform for biochemical interaction measurements, showing sensitivity values ranging from 2.3 to 3.3 p.m./nM for the particular case of thrombin detection.

1. Introduction

There is a growing interest in optical fiber sensors over the last decades, being considered as a high-performant approach for the identification of different analytes (McDonagh et al., 2008; Yin et al., 2018). Optical fibers act as light transducers and serve as an excellent platform to attach receptors and perform rapid and label-free detection of biomolecules (Wang and Wolfbeis, 2016). They exhibit significant advantages over other sensing technologies, such as cost-effectiveness, small size, flexibility, light weight, magnetic resonance compatibility or remote and multiplexed detection capability (Yin et al., 2018). In addition, optical fibers extend the possibility of performing detection in non-liquid media such as gel matrices and human tissues, as well as in hard to reach environments (Ribaut et al., 2017). Fiber optic biosensors have been widely studied for the detection of disease-related proteins (Albert et al., 2013a; Bekmurzayeva et al., 2018; Loyez et al., 2019b; Shevchenko et al., 2011; Sun et al., 2018), cancerous cells (Jian et al., 2019), small molecules (Allsop et al., 2019; Carrasquilla et al., 2011; Hu et al., 2018) and biofilm growth (Yuan et al., 2016).

In an optical fiber, light is confined in the core and is transmitted through total internal reflection with very low propagation loss. For biosensing applications, the fiber structure is modified in order to allow the interaction of light with the surrounding environment at the sensing point(s). Such modifications include chemical etching (Bekmurzayeva et al., 2018), tapering (Sun et al., 2018), polishing (Huang et al., 2018), bending (Gowri and Sai, 2016) and grating photo-inscription (González-Vila et al., 2017a). The first three methods alter the thickness of the cladding, whilst bending and grating photo-inscription allow to preserve the physical integrity of the optical fiber. Depending on the type of application, both sensitivity and applicability need to be

* Corresponding author. PI National Laboratory Astana, Laboratory of Biosensors and Bioinstruments, 53 Kabanbay Batyr Avenue, 010000, Nur-Sultan, Kazakhstan.
E-mail address: m.sypabekova@nu.edu.kz (M. Sypabekova).
[1] Present Addresses: Sanzhar Korganbayev has moved to Department of Mechanical Engineering, Politecnico di Milano, 1 Via Giuseppe La Masa, 20156, Milano, Italy.

https://doi.org/10.1016/j.bios.2019.111765
Received 16 August 2019; Received in revised form 1 October 2019; Accepted 3 October 2019
Available online 5 October 2019
0956-5663/

considered and hence the choice of modified fiber type. Another alternative is the use of photonic crystal fibers, in which the structure of the core allows the detection of analytes through the holes of the fiber (Rifat et al., 2017).

In biosensing, the surface of the modified fiber is usually functionalized with a specific type of receptor which can only bind to a certain analyte. Therefore, the interaction of light with the medium surrounding the fiber depends on the biochemical reaction taking place on the fiber surface. In order to enhance the response in the form of refractive index (RI) change, absorption or conductivity, the fiber surface is usually covered with functional materials such as gold nanofilms (Caucheteur et al., 2016), nanoparticles (Lepinay et al., 2014), carbon nanotubes (Parveen et al., 2017), graphene (Chiu et al., 2017), metal oxides (L Coelho et al., 2016)and polymers (Yin et al., 2016). Receptors such as aptamers and antibodies are usually immobilized on the functional material on the surface of the fiber and altogether allow to sense biomolecules down to pM level (Ribaut et al., 2016).

Amongst modified fibers, grating-based optical fiber sensors such as tilted fiber Bragg gratings (TFBGs) have been extensively studied for biomolecule detection. TFBG sensors provide simple and robust platforms for bioreceptor attachment and consequent detection. They have been effectively applied to a wide range of target analytes (Loyez et al., 2019b, 2019a; 2018; Zhou et al., 2019). The sensing mechanism used in TFBG fiber-optic biosensors is based on the excitation of forward-propagating cladding modes able to reach the interface between the cladding and the outer medium. These modes are sensitive to RI changes in the medium surrounding the optical fiber and their optical response consists of a simultaneous wavelength shift and amplitude variation (González-Vila et al., 2017b). In several published works, TFBG fiber-optic biosensors profit from the surface plasmon resonance (SPR) phenomenon to enhance their bulk sensitivity (Chiavaioli et al., 2017) through the use of a thin-film metal coating (Loyez et al., 2019c). The generation of metal nanoparticles has also been exploited, requiring important parameter management including the size and the shape of the particles (Shao et al., 2011). Therefore, with the advances in surface chemistry research, the use of non-plasmonic functionalized TFBGs becomes an interesting approach as well for biodetection purposes (Bekmurzayeva et al., 2018). Indeed, recent studies showed the feasibility of using non-metallic coated surfaces for the covalent immobilization of the bioreceptors with high quality factor of the spectrum resonances (Loyez et al., 2018), bypassing the conductive layer deposition on the fiber surface.

With regard to chemical etching, several works have studied the influence of cladding etched FBGs on the RI sensitivity (da Fonseca et al., 2011; Shivananju et al., 2013; Yun et al., 2007). Particularly, wet etching in HF (hydrofluoric acid), is commonly used in mass production of electronic circuitry and therefore it is compatible with high-volume manufacturing (Spierings, 1993). This process is usually done by immersing a section of the optical fiber in the etching solution during a few minutes at a controlled rate, in order to partially remove its cladding. The fabrication of such sensors is relatively fast and straightforward and offers simple tunability of the sensitivity (Bekmurzayeva et al., 2018). The detection in such configurations is done by analyzing the spectral changes in both transmission and reflection, without the need for polarization control (Bekmurzayeva et al., 2018).

In this work, we combine two fiber modifications, namely fiber grating photo-inscription and chemical etching, in order to provide a TFBG-based biosensor with enhanced sensitivity. We describe a process in which the fiber thickness can be easily tuned and hence the sensitivity of the platform. Unlike other TFBG-based biosensors that work in transmission, the current work is based on reflection measurements and avoids the use of external polarization controllers. For the immobilization of bioreceptors, simple surface chemistry based on silane-coupling agents was used directly on the fiber cladding. We study the effect of chemical etching on the sensitivity of the TFBG sensor and demonstrate the possibilities for biomolecule detection. First, the TFBGs were chemically etched and calibrated with different RI solutions (from 1.3418 to 1.4419 RIU). When coarsely interrogated, the etched tilted fiber Bragg gratings (eTFBGs) show an improved sensitivity up to 23.38 nm/RIU as compared to the original TFBGs, around 1.25 nm/RIU. Subsequently, the fiber was functionalized with thrombin aptamer, a widely used aptamer in biosensing studies, for the detection of thrombin in different concentrations, resulting surface sensitivity values between 2.3 and 3.3 p.m./nM.

2. Material and methods

2.1. Chemicals

(3-Aminopropyl)triethoxysilane (APTES), glutaraldehyde, phosphate-buffered saline (PBS), thrombin protein, hydrogen peroxide (H_2O_2), hydrofluoric acid (HF) and sulfuric acid (H_2SO_4) were purchased from Sigma Aldrich (Darmstadt, Germany). D-Sucrose, sodium dodecyl sulfate (SDS) and bovine serum albumin were obtained from Thermo Fisher Scientific (Runcorn, UK). Absolute ethanol was purchased from Aidabul Distillery (Kokshetau, Kazakhstan). Amine-modified thrombin binding aptamer (5^0-AmC_6-TTTTT-AGTCCGTGG-TAGGGCAGGTTGGGGTGACT-3^0) was synthesized by Sigma Aldrich. All aqueous solutions were prepared using 18.2 MΩcm ultra-pure water with a Pyrogard filter (Millipore, UK). Protein solutions were prepared freshly each time in 10 mM PBS at pH 7.4.

2.2. TFBG photo-inscription

1 cm long 10° TFBGs were photo-inscribed in the core of a hydrogen-loaded photosensitive single-mode optical fiber (PS-1250 from Fibercore UK) using the phase-mask technique (Hill et al., 1993). The photo-inscription setup consisted in an excimer ArF laser emitting at 193 nm, being part of a Noria FBG Manufacturing System (NorthLab Photonics) and a custom phase-mask providing a tilted holographic pattern with a pitch of 1078 nm. The laser energy was set to 5 mJ and the repetition rate to 50 Hz, requiring 3 bursts of 7500 pulses for each TFBG. TFBGs fabricated following this procedure exhibit a broad range of cladding mode resonances, being suitable to be used both in aqueous and gaseous media (González-Vila et al., 2018).

2.3. TFBG interrogation

The setup used for the development and interrogation of the biosensor is shown in Fig. 1. The peak wavelength shift and the reflection spectra of the eTFBGs were measured using an Optical Backscatter Reflectometer (OBR 4600, Luna Inc.) with a resolution of 8 p.m., a wavelength window between 1530 and 1616.4 nm and operating in distributed sensing mode at a speed of 3 Hz. The interrogator was used for the interrogation of the eTFBG spectra throughout calibration, fabrication and functionalization steps, as well as for the detection during thrombin measurements.

2.4. TFBG chemical etching and RI calibration

The output of the OBR was connected to the TFBG through an SMF (single-mode fiber) pigtail. The other end of the TFBG was spliced to a gold reflector (Luna Inc.). The gold reflector was used to visualize the reflection of the TFBG transmission spectrum and it was not linked to the generation of surface plasmon resonance (SPR) signal. Instead, this work bypasses the use of metal coatings around the TFBG sensing region and hence SPR signal generation. Both fibers were spliced to the TFBG using a standard splicer (Fujikura 12-S, SMF-SMF splicing mode). The TFBG was etched by immersing the grating region (approx. 1–2 cm) in a solution of 48% HF. The etching process, sketched in Fig. 1, was performed by incubating the TFBG in the HF bath under the chemical laminar hood (Waldner Secuflow airflow controller, ceiling-bench mounted) at room

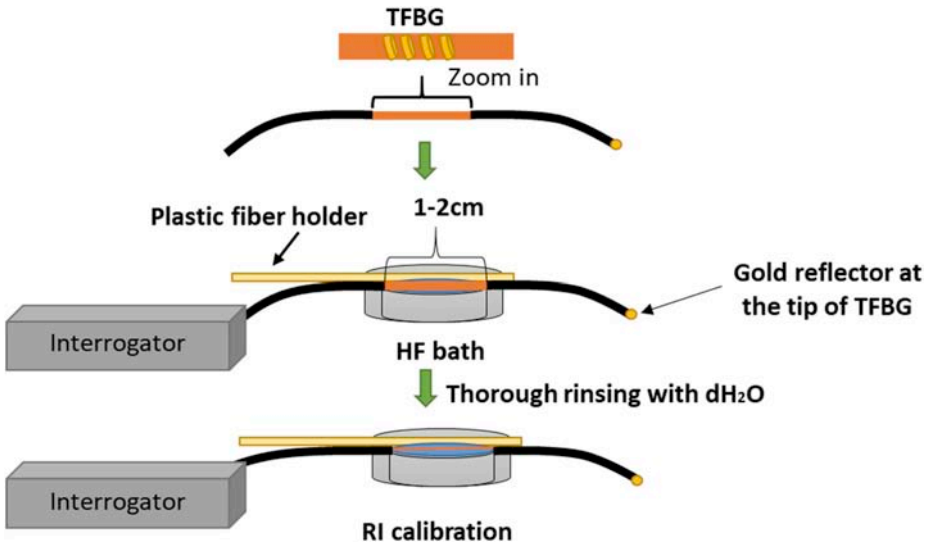

Fig. 1. Schematic overview of the etching process.

temperature. After each etching process the fiber was rinsed thoroughly with dH2O several times to remove remaining HF residues. Sucrose solution was used for the preparation of solutions with varying RI from 1.3418 to 1.4419 RIU. The RI of each solution was measured using an automatic digital refractometer (Anton Paar, Inc., Abbemat 300). TFBG and eTFBG calibration with varying RI was performed by completely immersing the grating region in 2.5 ml of sucrose solutions. The wavelength shift was measured using the leftmost cladding mode resonances visible on the window of the interrogator. The TFBG remained in the sucrose solution for at least 10–15 s before recording the measurement with the OBR. The diameter of the fiber was estimated by measuring the spectral shift of the Bragg wavelength during the etching process (Bekmurzayeva et al., 2018).

2.5. Fiber surface functionalization and thrombin detection

The surface of the fiber was functionalized with the thrombin aptamer as described in (Bekmurzayeva et al., 2018) with some modifications, as it is shown in Fig. 2. Briefly, the fiber was first cleaned using piranha solution (1:3 vol ratio H2SO4: H2O) for 10 min followed by thorough rinsing with dH2O. It was further incubated in 5% APTES in absolute ethanol for 30 min followed by rinsing with ethanol. The fiber was then placed at 110 °C in an oven for another 30 min followed by further incubation in 25% glutaraldehyde in 10 mM PBS for 1 h. After glutaraldehyde, the fiber was rinsed with dH2O and incubated in 1 μM thrombin aptamer solution in 10 mM PBS for at least 2 h at room temperature. The fiber surface was washed with 0.2% SDS in 10 mM PBS followed by thorough sensing with 10 mM PBS to remove any of the remaining SDS molecules from the fiber surface. 1% BSA was used as blocking reagent and allowed to incubate for 30 min followed by rinsing

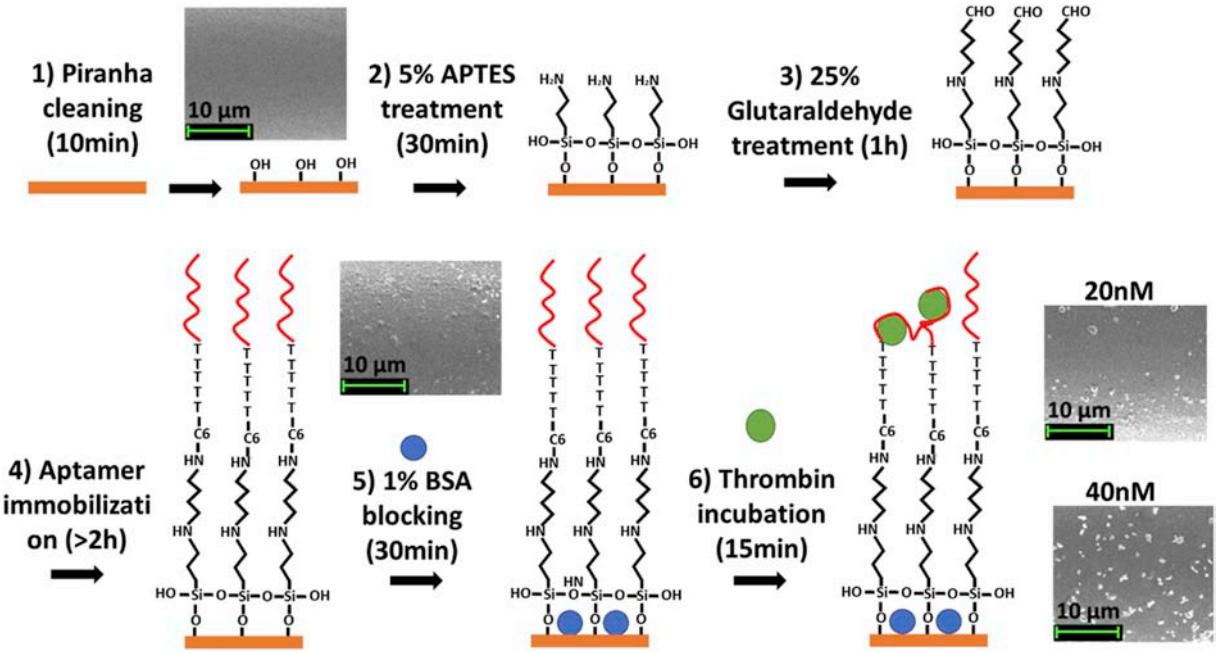

Fig. 2. Schematic overview of the functionalization of the eTFBG with thrombin aptamer and thrombin detection. SEM images for clean, aptamer immobilized fiber surface and after thrombin detection (20 nM, 40 nM).

with 10 mM PBS. Different concentrations of thrombin molecule dissolved in 10 mM PBS (40 nM, 20 nM, 10 nM, 5 nM, 2.5 nM, 1.25 nM and 0.625 nM) allowed to interact with the fiber surface for 15 min followed by rinsing with 10 mM PBS and measurement of the spectra in 10 mM PBS.

2.6. Microscopy analysis

The functionalized optical fiber was analyzed by Scanning Electron Microscope (SEM, FeSEM Auriga, Crossbeam 540) and a Leica DM4000 B Digital Microscope with 20x/0.50 objective. The HF etching and functionalization procedures were the same as in section 2.4 and 2.5 respectively. At the end of each step, the fiber was thoroughly rinsed with dH_2O (piranha cleaning) and 10 mM PBS (aptamer immobilization and thrombin detection) and allowed to air-dry overnight. 1 cm of functionalized optical fiber was then cleaved and glued onto the stubs. For the SEM analysis the samples were gold-sputtered with an automatic sputter coater (Quorum, Q150T) at 2 nm thickness. The functionalized fibers were then observed at different magnifications under SEM (gold sputtered fibers) and under digital microscope. Images were taken for clean fiber surface, aptamer immobilized fiber, and after thrombin (20 nM, 40 nM) incubation.

3. Results and discussion

3.1. Influence of chemical etching on the TFBG sensitivity

The main aim of our experimental work is to study the effect of the chemical etching of the TFBGs on their sensitivity. In order to do that, TFBGs with a tilt angle of 10° and a diameter of 125 μm were etched stepwise with HF solution and the corresponding spectra were recorded. In each step, the measurements were carried out in ultrapure water and then the TFBGs were allowed to be etched further in HF solution. The fiber diameter was estimated by measuring the wavelength shift of the Bragg mode (Bekmurzayeva et al., 2018) and it was reduced from 125 μm to 13 μm with increasing etching time, resulting in the spectral evolution seen in Fig. 3. From the original reflection spectra (125 μm, blue), the enlarged bandwidth was observed during the etching process as a consequence of the mode escaping to the surrounding medium. Enlarged bandwidth refers to the fact that during the etching process, the wavelength span between the m-th and the (m+1)-th cladding mode was increased as visible in Fig. 3, as a consequence of the thinner

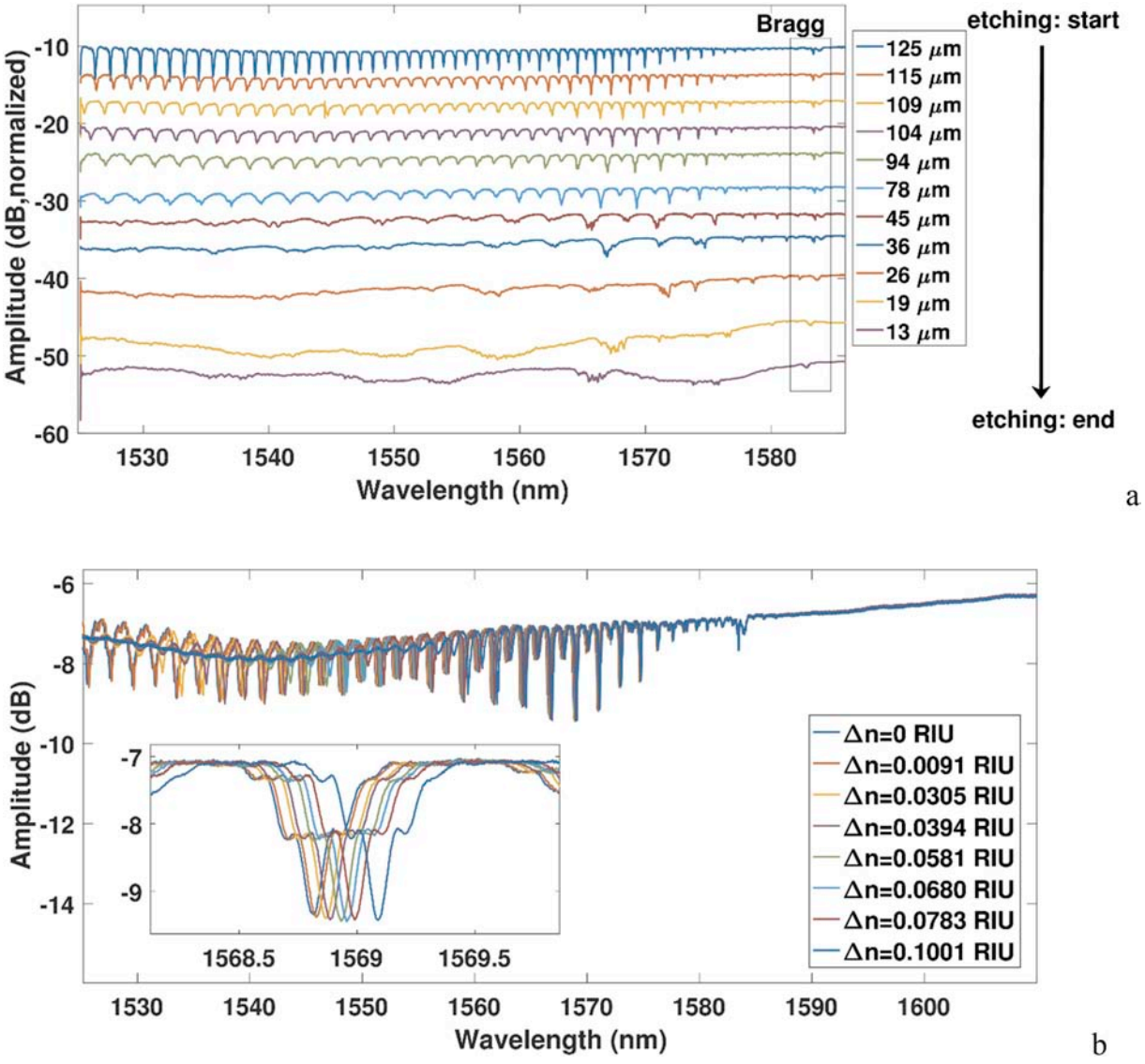

Fig. 3. (a) Reflection spectra throughout the HF etching of the TFBG; (b) Spectral change of the eTFBG (d = 94 μm) for different sucrose concentrations; inset: zoom on the modes where the analysis was carried out.

cladding diameter. Thus, when looking at the overall eTFBG "transmission-reflection" spectrum, as etching progressed the spectrum of the device was enlarged towards the shorter wavelengths.

To quantify the sensitivity of the eTFBG to RI variations, TFBGs (reference) and eTFBGs were immersed into a sucrose solution with controlled RI variations with a digital refractometer. We analyzed modes near 1569 nm as this wavelength allows observation for all investigated RI variations and diameters. Fig. 3b illustrates the spectral change of the eTFBG (94 μm fiber diameter) corresponding to different sucrose concentrations. Fig. 3b **(inset)** focuses on the spectral change of the eTFBG for the modes between 1568.5 and 1569.5 nm. The wavelength shifts of these modes for each sucrose concentration as a function of the surrounding refractive index change are shown in Fig. 4. The wavelength change was calculated using the lower peak of the mode. The sensitivity to surrounding RI variations was determined as the ratio between the wavelength shift observed in the eTFBG and the change of refractive index. Fig. 4 **inset** shows the calculated sensitivity values corresponding to increasing etching times for TFBGs (blue, 125 μm fiber diameter) and different eTFBGs, as the etching time progresses and the fiber diameter, consequently, gets thinner. According to the graph, the sensitivity to RI variations was increased with increasing etching time, i.e. 23.38 nm/RIU for e-TFBG (d = 13 μm) and 1.25nm/RIU for the TFBG (d = 125 μm) for RI variations between 1.3418 and 1.4419. Previous work on un-etched TFBGs showed that the sensitivity was 20–25 nm/RIU. However, the sensitivity was established for a smaller RI range (1.373–1.370) (Caucheteur et al., 2018) and it was based on measuring the most sensitive mode at the RI range of interest. In this work, the TFBG was etched and this process affected the spectrum by acting on the cladding modes separation. The mode to be tracked was selected in terms of sensitivity (quantitative nm/RIU value at the larger RI range) and persistence (i.e. the mode is always located on the interrogation window and never falling below cut-off), such that the mode is reliable for operation of the device. At a single wavelength of analysis, the sensitivity at 1.3418–1.4419 values of RI increased with etching. It should be noted that the etching rate is mostly dependent on the quality of the HF solution and on the experimental setup (sealed or open container), therefore the estimation of the fiber diameter during the etching process was considered rather than the etching time. At the end of the etching process the fiber diameter became extremely thin making it difficult to further manipulate during functionalization steps. Therefore, for biosensing applications (thrombin detection) we stopped etching once the fiber diameter was relatively thick enough (94 μm ≥ d ≥ 45 μm) to be suitable and applicable for the following functionalization steps.

3.2. Thrombin detection with eTFBGs

As it was shown the sensitivity of an eTFBG was higher than that of an un-etched TFBG and it increased with an increasing etching rate and decreasing the fiber diameter. Therefore in order to show the "optics of the device" and its potential application as opposed to the application and device, the biosensitivity was further tested to validate the sensing properties of the eTFBG using aptamer as a bioreceptor and thrombin molecule as a target. Thrombin is a 72 kDa protein, which plays an important role in the blood coagulation process (Liu et al., 2017). It is involved in atherosclerosis, thromboembolic and inflammatory disease (Li et al., 2016). Thrombin levels are elevated in cancer disease and hence the detection of the protein in blood has drawn increased attention (Falanga and Marchetti, 2018). The detection of thrombin using biosensors of different types (Coelho et al., 2014; Shevchenko et al., 2011; Sun et al., 2014) is based mostly on the interaction with the synthetic receptor-aptamer. Aptamers are single-stranded oligonucleotides that can bind to a target with high affinity and specificity. We used a 29mer thrombin aptamer (TBA) initially selected by (Tasset et al., 1997) with an equilibrium dissociation constant $K_D = 100$ nM.

The TBA aptamer was attached to the fiber surface based in a salinization process, with the help of silane-coupling agents (Bekmurzayeva et al., 2018), thus bypassing the use of a metal deposition. We used a silane-coupling agent (APTES) and a cross-linking agent (glutaraldehyde) for the immobilization of TBA on the eTFBG surface, as shown in Fig. 2.

A SEM study of the functionalized fiber surface was performed to characterize its morphology. The surface of the fiber after cleaning with piranha solution, after aptamer immobilization step and after thrombin incubation were tested to investigate the impact of each step. As can be seen in Fig. 2, the surface after the cleaning step was smooth without roughness. Small perturbations started to form after the aptamer immobilization step. Spherical shaped forms were observed on the surface incubated with 20 nM thrombin. With an increasing thrombin concentration at 40 nM, the number of spherical forms increased possibly indicating the thrombin attachment onto the aptamer-functionalized fiber surface. Fig. 5 shows the different stages of the eTFBG thrombin biosensor fabrication under the digital microscope. As it can be seen, the fiber diameter decreased after the etching with HF.

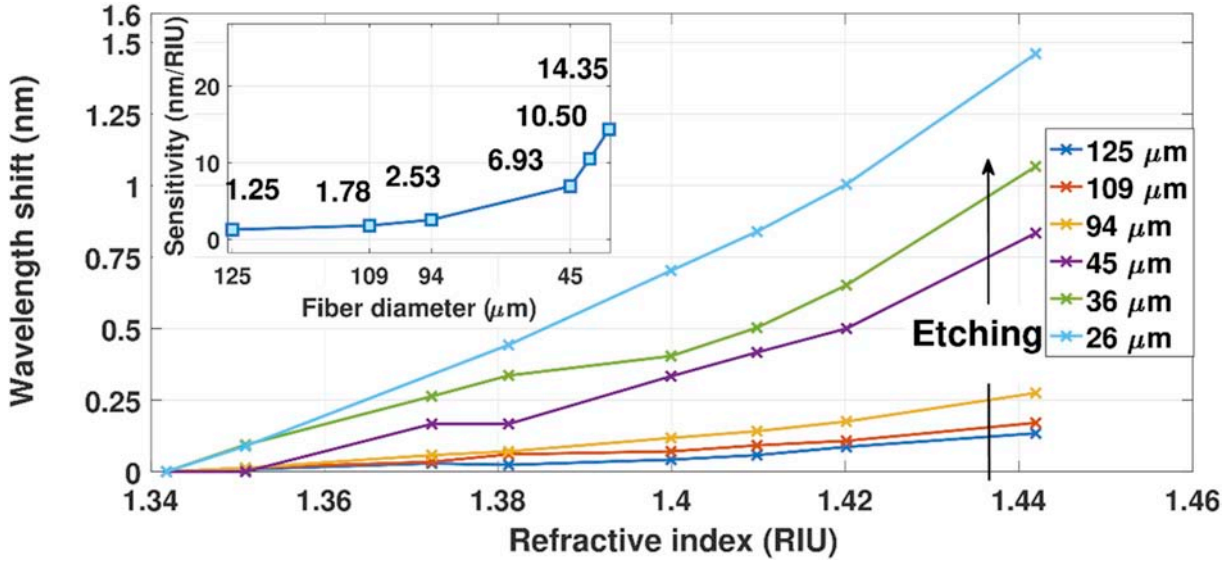

Fig. 4. Calibration curve of the eTFBG, reporting the wavelength shift as a function of the refractive index value for different values of fiber diameter. The inset shows the sensitivity as a function of the etching time.

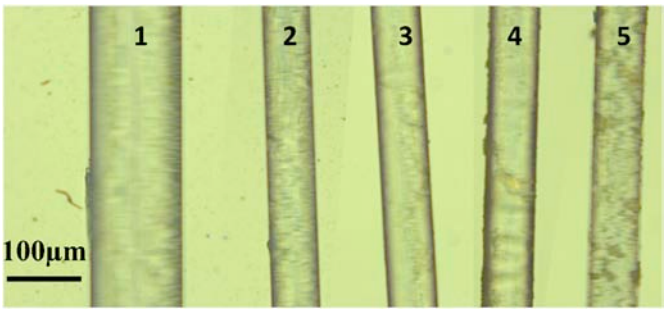

Fig. 5. Microscopy images of the eTFBG biosensor at different fabrication stages. 1: TFBG; 2: eTFBG; 3: eTFBG with thrombin aptamer; 4: eTFBG with 20 nM thrombin; 5: eTFBG with 40 nM thrombin. Images taken by a Leica DM4000 B Digital Microscope with 20x/0.50 objective.

Both Figs. 5 and 2 showed that the size and the number of perturbations increased with the increase of thrombin concentrations indicating a successful binding of thrombin onto the aptamer functionalized eTFBG biosensor.

For the protein detection we used eTFBG with sensitivity of 2.53 nm/RIU and with d = 94 µm. The biosensing responses were studied using different concentrations of thrombin, ranging from 2.5 to 40 nM to prove the concept that the biodetection indeed influences the wavelength shift generated from the binding process. The sensor response was monitored using the cladding modes between 1526.0 and 1529.1 nm, as it can be seen in Fig. 6a. The inset of this figure shows the spectra of the leftmost mode 1 at around 1526 nm. The arrow indicates the wavelength shift from the lowest to the highest thrombin concentrations studied, which indicates a red shift with increasing thrombin concentration. Fig. 6b shows the wavelength shift measured at different concentration of thrombin, for the 3 modes in proximity of the leftmost part of the detection window. We analyzed the response of multiple modes, in order to verify the robustness of the detection method (i.e. not only one mode responds) and hence showed that all the grating made the detection reliable. The stability measured the amount of wavelength shift observed at each concentration, after the wavelength has stabilized (i.e. the fluctuations of each point in Fig. 6b). This range fluctuated from -0.44 to +0.45 p.m. for the measurements. Conversely, the Bragg

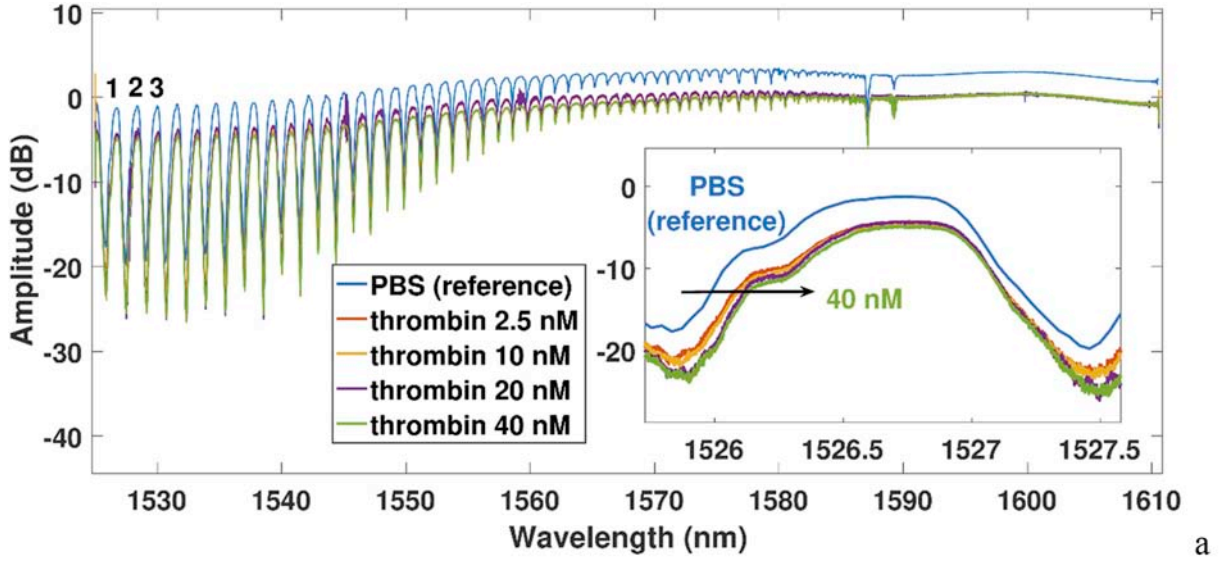

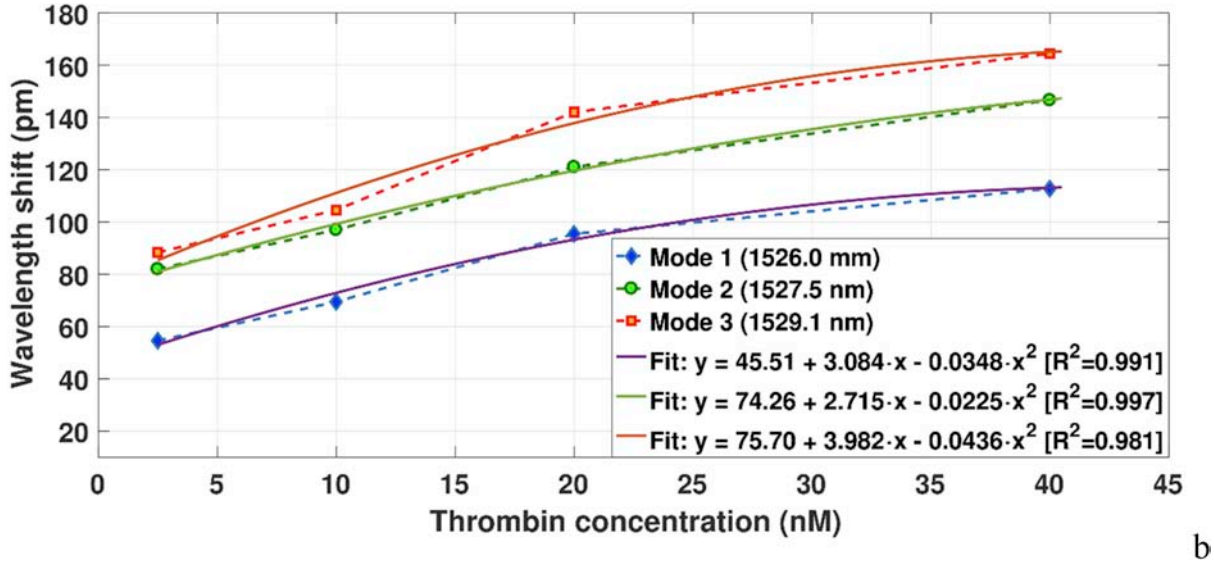

Fig. 6. a) Reflection spectra during the detection of different thrombin concentrations (2.5 nM, 10 nM, 20 nM and 40 nM). b) Wavelength shift (measurement in PBS considered as a reference) as a function of the thrombin concentration for the 3 most sensitive modes. Error bar range: -0.44 to +0.45 p.m.

wavelength of the eTFBG (insensitive to refractive index changes) had a fluctuation of ± 0.04 p.m. during the experiments, which confirms that the fluctuations on Fig. 6b are attributable to the RI change. The accuracy was measured by calculating the root mean square error (RMSE) of peak tracking at constant RI and constant temperature, and over long term it was estimated at ± 0.3 p.m.. This result is in agreement with (Tosi, 2017) where a 0.2 p.m. RMSE was estimated for similar values of signal-to-noise ratio at detector. Overall, we can infer therefore that the stability and accuracy have similar values. The relative standard deviation in the range 2.5–40 nM can be therefore estimated as

$$\frac{9pm}{90.7pm} \times 100\% \cong 1.0\%$$

(i.e. standard deviation of detected values divided by mean wavelength shift * 100%). The results are similar for several modes. An important factor contributing to the low fluctuation is the very accurate wavelength stability of the OBR interrogator, which is «0.1 p.m. due to the wavelength cell stabilization process through a gas cell, which allows a very precise measurement of wavelength shift.

We observed a trend almost quadratic for the detection, with a quadratic term relatively small (Fig. 6 **inset**). The relationship can be inverted in order to estimate thrombin concentration from wavelength shift. The linear fitting resulted in surface sensitivities for modes 1, 2, and 3 equal to 2.3 p.m./nM, 2.8 p.m./nM and 3.3 p.m./nM respectively. The accuracy (standard deviation: SD) for a wavelength shift was ~0.1 p.m. using spline method (Tosi, 2017). The LoD for mode 1 was estimated theoretically based on Fig. 6b:

$$y\ [pm] = 45.51 + 3.084x - 0.0348x^2.$$

The second order term ($0.0348x^2$) was neglected and the approximate conversion was 3.084 p.m./nM. In order to consider a reliable detection the SD was multiplied by 3 (0.3 p.m.). Hence the theoretical LOD can be estimated as follows:

$$LoD(mode\ 1) = \frac{0.3\ [pm]}{3.084\ [pm/nM]} = 0.097[nM]$$

The same method was applied to estimate the theoretical LoD for modes 2 and 3 and was found to be 0.110 nM and 0.075 nM, respectively. These values are about one order of magnitude lower than the ones previously reported with fiber gratings (Table 1) for the particular case of thrombin detection. Most of the works in Table 1 exploit the SPR phenomenon for the detection which requires the deposition of a thin metal film (gold-Au) on the sensing area of the fiber (Albert et al., 2013a; Luís Coelho et al., 2016; Shevchenko et al., 2011). The deposition of a thin metal film often requires perfect cleaning and precisely controlled homogenous metal deposition with uniform thickness (Loyez et al., 2018; Suzuki et al., 2008). The above mentioned parameters are important to control since they affect the sensitivity of the biosensor. The use of nanoparticles on gold coated fibers to generate localized SPR enhances the sensitivity of the biosensor (Lao et al., 2019), however the diameter and shapes of the nanoparticles as well as the metal deposition in this case requires precise control and instrument calibration. Other study eliminated the use of intermediate conductive layer deposition on fiber surfaces, thereby avoiding SPR excitation. The shape of the fiber was altered by tapering, which requires the use of high temperatures or laser sources and controlled motors to pull the fiber at both ends (Sun et al., 2018). The procedure itself demands careful design and parameter optimization in addition to the thin fiber diameter, which could be difficult to work with during the functionalization steps. The sensitivity of such tapered fiber for thrombin detection was lower as compared to the grating-inscribed fibers coated with a thin metal layer. The work presented in this paper used simple surface chemistry based on silanization and relatively fast and straightforward controlled etching with HF to partially remove the cladding region of the fiber.

In a TFBG, or e-TFBG, the RI sensitivity is encoded in the cladding modes, while the core mode (located at the longest wavelength) is unaffected by RI changes. Temperature affects the whole spectrum, instead, with a sensitivity of ~10 p.m./K (10.2 p.m./K in the fiber used in our experiments, similar to most SMF fibers). In this case, as in (Albert et al., 2013b), the temperature change can be measured by the core (Bragg) mode wavelength shift, and compensated in the whole FBG. In experiments, the temperature change was indeed not perceivable, falling below the accuracy of the peak tracking method used to identify the wavelength shift of the eTFBG. In practical applications (e.g. in situ, long term monitoring), it is possible to estimate the RI and temperature change, jointly, by compensating the wavelength shift by the temperature change measured by the Bragg mode (considering that the sensitivity is approximately the same in the whole range of the interrogator). This method is acquainted in optics and biosensors, and can be used to compensate small temperature fluctuations e.g. body temperature change (Loyez et al., 2019a).

Overall this work is intended to serve as a proof of concept showing the capability of this modified optical platform to outperform grating-based configurations reported so far.

4. Conclusion

The effect that chemical etching has on the bulk sensitivity of TFBGs was studied. The results showed that the sensitivity of the eTFBG was increased with an increasing etching process. We calibrated the TFBG fiber at each etching step with a sucrose solution with varying RI from 1.3418 to 1.4419 RIU. At the beginning of the etching process, the sensitivity of the TFBG was 1.25 nm/RIU when being measured in a coarse manner. The increased etching process resulted in decreasing the overall fiber diameter from 125 μm down to 13 μm. The sensitivity of the TFBG fiber throughout the etching process increased exponentially and reached a maximum of 23.38 nm/RIU.

We then tested our setup for thrombin molecule detection in the range of clinically important values using a functionalized eTFBG. The technology used during the fabrication of the biosensor was simple, reliable and cost effective, not involving complex surface modification or metal deposition on the fiber surface. The sensor was first etched in a 48% HF solution, which increased its RI sensitivity. Then, the fiber was functionalized for selective thrombin sensing based in silane-coupling surface chemistry and through the immobilizing of the thrombin binding aptamer. Microscopy analysis of the modified surfaces showed increased roughness, suggesting successful modification of the surface after the aptamer immobilization. We observed a different shift of the Bragg wavelength for each concentration value for the leftmost 3 modes

Table 1
Comparison of previously reported biosensors based on fiber gratings for thrombin detection.

Aptamer sequence	Fiber type	Fiber surface modification	LoD	Ref.
HS–$(CH_2)_6$–5′GGT TGG TGT GGT TGG3′	TFBG	50 nm Au sheath	22 nM	(Albert et al., 2013c)
HS–$(CH_2)_6$–5′GGT TGG TGT GGT TGG3′	TFBG	50 nm Au sheath	22.6 nM	Shevchenko et al. (2011)
NH_2-5′GGTTGGTGTGGTTGG3′	LPG	2 nm Cr, 16 nm Au, 100 nm TiO2	10 nM	(Luís Coelho et al., 2016)
HS-$(CH_2)_6$–5′GGTTGGTGTGGTTGG-3′ HS–$(CH_2)_6$–5′AGTCCGTGGTAGGGCAGGTTG GGGTGACT3′	TFBG	Au sheath + Au nanoparticles	1 nM	Lao et al. (2019)
NH_2-5′GGTTGGTGTGGTTGG3′	Tapered	Silanization	0.1 μM	Sun et al. (2018)
NH_2-$(CH_2)_6$-5′GGT TGG TGT GGT TGG3′	etched TFBG	Silanization	0.075–0.110 nM	This work

visible on our interrogator with a maximum sensitivity of 3.3 p.m./nM with theoretical LoD between 0.110 nM and 0.075 nM. Therefore, we demonstrate that eTFBG platforms can be successfully used for biosensing purposes, aiming to exploit the advantages of these structures for biomolecule detection.

Funding sources

This work has been funded by ORAU program at Nazarbayev University (grant: LIFESTART; PI: Daniele Tosi). The research has been supported by NATO Science for Peace and Security program (grant G5486). Álvaro González-Vila and Christophe Caucheteur are supported by the Belgian F.R.S.-FNRS, also through the grant no. O001518F (EOS-convention 30467715).

Author contributions

The manuscript was written through contributions of all authors. All authors have given approval to the final version of the manuscript.

Declaration of competing interest

The authors declare that they have no known competing financial interests or personal relationships that could have appeared to influence the work reported in this paper.

CRediT authorship contribution statement

Marzhan Sypabekova: Conceptualization, Formal analysis, Investigation, Methodology, Validation, Writing - original draft, Writing - review & editing. **Sanzhar Korganbayev:** Data curation, Formal analysis, Software. **Álvaro González-Vila:** Methodology, Investigation, Writing - review & editing. **Christophe Caucheteur:** Supervision, Writing - review & editing. **Madina Shaimerdenova:** Project administration, Investigation. **Takhmina Ayupova:** Project administration, Investigation. **Aliya Bekmurzayeva:** Project administration, Investigation. **Luca Vangelista:** Supervision. **Daniele Tosi:** Conceptualization, Supervision, Funding acquisition, Formal analysis, Writing - review & editing.

References

Albert, J., Lepinay, S., Caucheteur, C., DeRosa, M.C., 2013. High resolution grating-assisted surface plasmon resonance fiber optic aptasensor. Methods 63, 239–254.

Albert, J., Shao, L.-Y., Caucheteur, C., 2013. Tilted fiber Bragg grating sensors. Laser Photonics Rev. 7, 83–108. https://doi.org/10.1002/lpor.201100039.

Albert, J., Shao, L., Caucheteur, C., 2013. Tilted fiber Bragg grating sensors Tilted fiber Bragg grating sensors. .

Allsop, T.D.P., Neal, R., Wang, C., Nagel, D.A., Hine, A.V., Culverhouse, P., Castañón, J. D.A., Webb, D.J., Scarano, S., Minunni, M., 2019. An ultra-sensitive aptasensor on optical fibre for the direct detection of bisphenol A. Biosens. Bioelectron. 135, 102–110.

Bekmurzayeva, A., Dukenbayev, K., Shaimerdenova, M., Bekniyazov, I., Ayupova, T., Sypabekova, M., Molardi, C., Tosi, D., 2018. Etched fiber Bragg grating biosensor functionalized with aptamers for detection of thrombin. Sensors 18, 4298.

Carrasquilla, C., Xiao, Y., Xu, C.Q., Li, Y., Brennan, J.D., 2011. Enhancing sensitivity and selectivity of long-period grating sensors using structure-switching aptamers bound to gold-doped macroporous silica coatings. Anal. Chem. 83, 7984–7991. https://doi.org/10.1021/ac2020432.

Caucheteur, C., Guo, T., Liu, F., Guan, B.-O., Albert, J., 2016. Ultrasensitive plasmonic sensing in air using optical fibre spectral combs. Nat. Commun. 7, 13371.

Caucheteur, C., Loyez, M., González-Vila, Á., Wattiez, R., 2018. Evaluation of gold layer configuration for plasmonic fiber grating biosensors. Opt. Express 26, 24154–24163.

Chiavaioli, F., Gouveia, C., Jorge, P., Baldini, F., 2017. Towards a uniform metrological assessment of grating-based optical fiber sensors: from refractometers to biosensors. Biosensors 7, 23.

Chiu, Y.-D., Wu, C.-W., Chiang, C.-C., 2017. Tilted fiber Bragg grating sensor with graphene oxide coating for humidity sensing. Sensors 17, 2129.

Coelho, Luís, Marques Martins de Almeida, J.M., Santos, J.L., da Silva Jorge, P.A., Martins, M.C.L., Viegas, D., Queirós, R.B., 2016. Aptamer-based fiber sensor for thrombin detection. J. Biomed. Opt. 21 https://doi.org/10.1117/1.jbo.21.8.087005, 087005.

Coelho, L., Queiros, R.B., Santos, J.L., Martins, M.C.L., Viegas, D., Jorge, P.A.S., 2014. DNA-Aptamer optical biosensors based on a LPG-SPR optical fiber platform for point-of-care diagnostic. In: Plasmonics in Biology and Medicine Xi. International Society for Optics and Photonics, 89570K.

Coelho, L., Viegas, D., Santos, J.L., De Almeida, J., 2016. Characterization of zinc oxide coated optical fiber long period gratings with improved refractive index sensing properties. Sens. Actuators B Chem. 223, 45–51.

da Fonseca, J.P.T., Gondek, J.T., Possetti, G.R.C., Muller, M., Luís, J., Kamikawachi, R.C., 2011. Optical sensor based on etched fiber Bragg gratings for assessment of biodiesel quality. In: 2011 SBMO/IEEE MTT-S International Microwave and Optoelectronics Conference (IMOC 2011). IEEE, pp. 458–460.

Falanga, A., Marchetti, M., 2018. Hemostatic biomarkers in cancer progression. Thromb. Res. 164, S54–S61.

González-Vila, Á., Debliquy, M., Lahem, D., Zhang, C., Mégret, P., Caucheteur, C., 2017. Molecularly imprinted electropolymerization on a metal-coated optical fiber for gas sensing applications. Sens. Actuators B Chem. 244, 1145–1151.

González-Vila, Á., Ioannou, A., Loyez, M., Debliquy, M., Lahem, D., Caucheteur, C., 2018. Surface plasmon resonance sensing in gaseous media with optical fiber gratings. Opt. Lett. 43, 2308–2311.

González-Vila, Á., Kinet, D., Mégret, P., Caucheteur, C., 2017. Narrowband interrogation of plasmonic optical fiber biosensors based on spectral combs. Opt. Laser. Technol. 96, 141–146.

Gowri, A., Sai, V.V.R., 2016. Development of LSPR based U-bent plastic optical fiber sensors. Sens. Actuators B Chem. 230, 536–543.

Hill, K.O., Malo, B., Bilodeau, F., Johnson, D.C., Albert, J., 1993. Bragg gratings fabricated in monomode photosensitive optical fiber by UV exposure through a phase mask. Appl. Phys. Lett. 62, 1035–1037.

Hu, W., Huang, Y., Chen, C., Liu, Y., Guo, T., Guan, B.-O., 2018. Highly sensitive detection of dopamine using a graphene functionalized plasmonic fiber-optic sensor with aptamer conformational amplification. Sens. Actuators B Chem. 264, 440–447.

Huang, Y., Zhu, W., Li, Z., Chen, G., Chen, L., Zhou, J., Lin, H., Guan, J., Fang, W., Liu, X., 2018. High-performance fibre-optic humidity sensor based on a side-polished fibre wavelength selectively coupled with graphene oxide film. Sens. Actuators B Chem. 255, 57–69.

Jian, A., Zou, L., Bai, G., Duan, Q., Zhang, Y., Zhang, Q., Sang, S., Zhang, X., 2019. Highly sensitive cell concentration detection by resonant optical tunneling effect. J. Light. Technol. 37, 2800–2806.

Lao, J., Han, L., Wu, Z., Zhang, X., Huang, Y., Tang, Y., Guo, T., 2019. Gold nanoparticle-functionalized surface plasmon resonance optical fiber biosensor: in situ detection of thrombin with 1 n·M detection limit. J. Light. Technol. 37, 2748–2755. https://doi.org/10.1109/JLT.2018.2822827.

Lepinay, S., Staff, A., Ianoul, A., Albert, J., 2014. Improved detection limits of protein optical fiber biosensors coated with gold nanoparticles. Biosens. Bioelectron. 52, 337–344.

Li, S., Zhang, D., Zhang, Q., Lu, Y., Li, N., Chen, Q., Liu, Q., 2016. Electrophoresis-enhanced localized surface plasmon resonance sensing based on nanocup array for thrombin detection. Sens. Actuators B Chem. 232, 219–225.

Liu, M., Li, J., Li, B., 2017. A colorimetric aptamer biosensor based on cationic polythiophene derivative as peroxidase mimetics for the ultrasensitive detection of thrombin. Talanta 175, 224–228.

Loyez, M., Albert, J., Caucheteur, C., Wattiez, R., 2018. Cytokeratins biosensing using tilted fiber gratings. Biosensors 8, 74.

Loyez, M., Larrieu, J.-C., Chevineau, S., Remmelink, M., Leduc, D., Bondue, B., Lambert, P., Devière, J., Wattiez, R., Caucheteur, C., 2019. In situ cancer diagnosis through online plasmonics. Biosens. Bioelectron. 131, 104–112.

Loyez, M., Lobry, M., Wattiez, R., Caucheteur, C., 2019. Optical fiber gratings immunoassays. Sensors 19, 2595.

Loyez, M., Ribaut, C., Caucheteur, C., Wattiez, R., 2019. Functionalized gold electroless-plated optical fiber gratings for reliable surface biosensing. Sens. Actuators B Chem. 280, 54–61.

McDonagh, C., Burke, C.S., MacCraith, B.D., 2008. Optical chemical sensors. Chem. Rev. 108, 400–422. https://doi.org/10.1021/cr068102g.

Parveen, S., Pathak, A., Gupta, B.D., 2017. Fiber optic SPR nanosensor based on synergistic effects of CNT/Cu-nanoparticles composite for ultratrace sensing of nitrate. Sens. Actuators B Chem. 246, 910–919.

Ribaut, C., Loyez, M., Larrieu, J.-C., Chevineau, S., Lambert, P., Remmelink, M., Wattiez, R., Caucheteur, C., 2017. Cancer biomarker sensing using packaged plasmonic optical fiber gratings: towards in vivo diagnosis. Biosens. Bioelectron. 92, 449–456.

Ribaut, C., Voisin, V., Malachovská, V., Dubois, V., Mégret, P., Wattiez, R., Caucheteur, C., 2016. Small biomolecule immunosensing with plasmonic optical fiber grating sensor. Biosens. Bioelectron. 77, 315–322.

Rifat, A.A., Ahmed, R., Yetisen, A.K., Butt, H., Sabouri, A., Mahdiraji, G.A., Yun, S.H., Adikan, F.R.M., 2017. Photonic crystal fiber based plasmonic sensors. Sens. Actuators B Chem. https://doi.org/10.1016/j.snb.2016.11.113.

Shao, L.-Y., Coyle, J.P., Barry, S.T., Albert, J., 2011. Anomalous permittivity and plasmon resonances of copper nanoparticle conformal coatings on optical fibers. Opt. Mater. Express 1, 128–137.

Shevchenko, Y., Francis, T.J., Blair, D.A.D., Walsh, R., DeRosa, M.C., Albert, J., 2011. In situ biosensing with a surface plasmon resonance fiber grating aptasensor. Anal. Chem. 83, 7027–7034.

Shivananju, B.N., Renilkumar, M., Prashanth, G.R., Asokan, S., Varma, M.M., 2013. Detection limit of etched fiber Bragg grating sensors. J. Light. Technol. 31, 2441–2447.

Spierings, G., 1993. Wet chemical etching of silicate glasses in hydrofluoric acid based solutions. J. Mater. Sci. 28, 6261–6273.

Sun, C., Han, Q., Wang, D., Xu, W., Wang, W., Zhao, W., Zhou, M., 2014. A label-free and high sensitive aptamer biosensor based on hyperbranched polyester microspheres for thrombin detection. Anal. Chim. Acta 850, 33–40.
Sun, D.D., Sun, L.-P., Guo, T., Guan, B., 2018. Label-free thrombin detection using a tapered fiber-optic interferometric aptasensor. J. Light. Technol.
Suzuki, H., Sugimoto, M., Matsui, Y., Kondoh, J., 2008. Effects of gold film thickness on spectrum profile and sensitivity of a multimode-optical-fiber SPR sensor. Sens. Actuators B Chem. 132, 26–33. https://doi.org/10.1016/j.snb.2008.01.003.
Tasset, D.M., Kubik, M.F., Steiner, W., 1997. Oligonucleotide inhibitors of human thrombin that bind distinct epitopes. J. Mol. Biol. 272, 688–698.
Tosi, D., 2017. Review and analysis of peak tracking techniques for fiber Bragg grating sensors. Sensors 17, 2368.
Wang, X.D., Wolfbeis, O.S., 2016. Fiber-optic chemical sensors and biosensors (2013-2015). Anal. Chem. 88, 203–227. https://doi.org/10.1021/acs.analchem.5b04298.
Yin, M.-J., Gu, B., An, Q.-F., Yang, C., Guan, Y.L., Yong, K.-T., 2018. Recent development of fiber-optic chemical sensors and biosensors: mechanisms, materials, micro/nano-fabrications and applications. Coord. Chem. Rev. 376, 348–392.
Yin, M., Huang, B., Gao, S., Zhang, A.P., Ye, X., 2016. Optical fiber LPG biosensor integrated microfluidic chip for ultrasensitive glucose detection. Biomed. Opt. Express 7, 2067–2077.
Yuan, Y., Guo, T., Qiu, X., Tang, J., Huang, Y., Zhuang, L., Zhou, S., Li, Z., Guan, B.-O., Zhang, X., 2016. Electrochemical surface plasmon resonance fiber-optic sensor: in situ detection of electroactive biofilms. Anal. Chem. 88, 7609–7616.
Yun, B., Chen, N., Cui, Y., 2007. Highly sensitive liquid-level sensor based on etched fiber Bragg grating. IEEE Photonics Technol. Lett. 19, 1747–1749.
Zhou, L., Liu, C., Sun, Z., Mao, H., Zhang, L., Yu, X., Zhao, J., Chen, X., 2019. Black phosphorus based fiber optic biosensor for ultrasensitive cancer diagnosis. Biosens. Bioelectron. 137, 140–147.